https://doi.org/10.5194/egusphere-2026-4762
Preprint. Discussion started: 25 August 2026

Accurate and high-resolution measurements of UTLS water vapor by balloon-borne laser absorption spectroscopy

Simone Brunamonti[1], Yann Poltera[2,3], Gonzague Romanens[4], Alex Weitnauer[1], Philipp Scheidegger[1], Adrianos Filinis[2,3], Alistair Bell[2,3], Giovanni Martucci[4], Frank G. Wienhold[5], Thomas Peter[5], Peter Oelsner[6], Ruud Dirksen[6], Alexander Haefele[4], Lukas Emmenegger[1], Gunter Stober[2,3] and Béla Tuzson[1]

[1]Empa, Laboratory for Air Pollution/Environmental Technology, Dübendorf, Switzerland
[2]University of Bern, Institute of Applied Physics, Bern, Switzerland
[3]Oeschger Center for Climate Change Research, University of Bern, Bern, Switzerland
[4]Federal Office of Meterology and Climatology (MeteoSwiss), Payerne, Switzerland
[5]ETH Zürich, Institute for Atmospheric and Climate Science, Zürich, Switzerland
[6]Deutscher Wetterdienst/GRUAN Lead Center, Lindenberg, Germany

Correspondence to: Simone Brunamonti (simone.brunamonti@empa.ch) and Béla Tuzson (bela.tuzson@empa.ch)

Abstract. Accurate and sustained monitoring of water vapor (H_2O) in the upper troposphere-lower stratosphere (UTLS) is essential for quantifying its role in the atmospheric radiative balance, chemistry, and climate variability. However, in situ measurements in this region remain challenging due to the extremely low H_2O concentrations, harsh environmental conditions, and strict payload limitations on meteorological balloon platforms. ALBATROSS is a compact (3.6 kg), balloon-borne mid-infrared laser absorption spectrometer developed to provide highly accurate, SI-traceable H_2O measurements with high vertical resolution in the UTLS. Following recent comprehensive laboratory characterization, we present the first in-flight validation of ALBATROSS, based on seven balloon flights conducted between 2022 and 2026 from the meteorological observatories of Payerne, Switzerland (six flights) and Lindenberg, Germany (one flight). All flights included simultaneous measurements by a cryogenic frostpoint hygrometer (CFH) and a meteorological radiosonde (Vaisala RS41), with CFH operating either in a tandem-flight configuration or on the same payload as ALBATROSS. In the troposphere (up to 12 km altitude), the ALBATROSS retrieval agrees with both reference instruments within a mean relative difference of –2 ± 7 % with respect to RS41 and –1 ± 8 % with respect to CFH over nearly three orders of magnitude in H_2O mixing ratio. Fine-scale vertical structures and cirrus cloud layers are consistently resolved. In the stratosphere, following the implementation of an in-flight purging system to eliminate contamination from internal moisture sources, ALBATROSS achieves an agreement of 3 ± 10 % relative to CFH between 12 and 28 km altitude. An important advantage of laser absorption spectroscopy is demonstrated through observations of balloon-induced H_2O spikes detected simultaneously by ALBATROSS and CFH in the stratosphere. These measurements reveal fast dynamic response of the laser spectrometer of ~1 s, corresponding to an effective vertical resolution of 5 m, compared to 3–4 s (15–20 m) for frostpoint hygrometry. Overall, these results demonstrate the robust performance of ALBATROSS under real atmospheric conditions and establish mid-infrared laser absorption spectroscopy as a reference-quality technique for balloon-borne observations and long-term monitoring of UTLS H_2O.

https://doi.org/10.5194/egusphere-2026-4762
Preprint. Discussion started: 25 August 2026

1. Introduction

Water vapor (H_2O) is the strongest natural greenhouse gas in the Earth's atmosphere and plays a central role in atmospheric dynamics, cloud microphysics, and radiative transfer (Forster et al., 2021). Its concentration decreases with altitude from a few percent near the surface to only a few µmol mol^{-1} (i.e., parts per million, ppm) in the stratosphere. Despite this low abundance, H_2O in the upper troposphere-lower stratosphere (UTLS, ~8–25 km altitude) exerts a large impact on the radiative balance of the atmosphere (Solomon et al., 2010; Riese et al., 2012) and affects large-scale circulation (Maycock et al., 2014) and ozone chemistry (Stenke and Grewe, 2005).

The importance of accurately quantifying UTLS water vapor has been underscored by the January 2022 eruption of the submarine Hunga Tonga-Hunga Ha'apai volcano, which injected an unprecedented amount of water vapor into the stratosphere. This event increased the global stratospheric H_2O mass by more than 10 % relative to climatological levels and is expected to persist for several years, potentially inducing long-lasting climatic effects (Vömel et al., 2022; Khaykin et al., 2022). Therefore, high-accuracy and sustained measurements of UTLS H_2O are essential for monitoring the temporal evolution of this perturbation and for assessing its long-term climatic consequences.

Satellite instruments provide global observations of UTLS H_2O with extensive spatial and temporal coverage and a typical vertical resolution of 1.5–3 km (e.g., Hegglin et al., 2013; Santee et al., 2017). However, the continuity of these measurements is increasingly uncertain (Salawitch et al., 2025), and their vertical resolution is insufficient to resolve the fine-scale structures associated with UTLS processes such as dehydration near the tropopause and thin cirrus formation, which frequently occur on vertical scales of tens to hundreds of meters (e.g., Luo et al., 2003; Reinares Martínez et al., 2020).

High-resolution, in situ observations of UTLS H_2O are obtained using instruments deployed aboard weather balloons or high-altitude aircraft. While aircraft measurements can deliver high-quality data, they are typically limited to relatively short and sparse field campaigns (e.g., Rollins et al., 2014; Singer et al., 2022), In contrast, lightweight balloon-borne systems (payload < 4 kg) can provide routine measurements with vertical resolutions of a few meters and are suitable for long-term monitoring (e.g., Hurst et al., 2011) and satellite validation (Hurst et al., 2014; 2016). Balloon soundings are a fundamental component of ground-based global climate monitoring networks, such as the GCOS Reference Upper air Network (GRUAN) and the Network for the Detection of Atmospheric Composition Change (NDACC).

Within these networks, balloon-borne measurements of UTLS H_2O have traditionally relied on chilled-mirror frostpoint hygrometers, including the commercial cryogenic frostpoint hygrometer (CFH; EnSci, USA) (Vömel et al., 2007; 2016) and the NOAA frostpoint hygrometer (FPH) (Hall et al., 2016). These instruments have served as reference standards for decades (e.g., Oltmans et al., 2000; Fahey et al., 2014). However, ongoing technical developments highlight the need for complementary and independent measurement approaches.

First, the progressive phase-out of trifluoromethane (HFC-23) as a cooling agent, due to its high global warming potential (UNEP, 2016), has triggered the development of alternative cooling concepts, such as Peltier-based systems (Jorge, 2020; Sugidachi et al., 2025) and refrigerant mixtures based on dry ice or liquid N_2 (e.g., Rolf et al., 2020; Dirksen, 2024), whose

https://doi.org/10.5194/egusphere-2026-4762
Preprint. Discussion started: 25 August 2026

performance across the full range of atmospheric conditions has not yet been established. Second, chilled-mirror hygrometers are intrinsically affected by nonequilibrium effects arising from the finite response time of the mirror temperature controller, which can introduce errors exceeding ±10 % in H_2O mixing ratio under rapidly changing atmospheric conditions, and require dedicated post-processing procedures (Poltera et al., 2026). These limitations become increasingly relevant considering the recently updated GCOS requirements for UTLS H_2O observations, which set uncertainties as low as 0.1 ppm (~2 %) at 10 m vertical resolution as ultimate goal (GCOS, 2025). Altogether, this motivates the investigation of independent measurement techniques that combine high accuracy, rapid response, long-term stability, and traceability.

Several alternative methods for UTLS H_2O measurements aboard lightweight balloon platforms have been demonstrated, yet each exhibits intrinsic limitations. Thin-film polymer sensors (e.g., Survo et al., 2014), widely used in operational radiosondes, lose sensitivity at low relative humidity, and lack the accuracy, stability, and traceability required in the dry UTLS (Brunamonti et al., 2019). Lyman-α fluorescence hygrometers (e.g., Zöger et al., 1999) are limited by calibration complexity and long-term stability issues (Meyer et al., 2015). In contrast, laser absorption spectroscopy (e.g., Durry et al., 2008; Ghysels et al., 2016; 2024; Graf et al., 2021) offers a particularly promising pathway by combining high accuracy and precision, fast response, and a direct spectroscopic retrieval traceable to fundamental molecular parameters.

The ALBATROSS spectrometer (Graf et al., 2021) was developed to provide highly accurate, SI-traceable H_2O measurements with high vertical resolution in the UTLS aboard meteorological balloon platforms, thus addressing the emerging UTLS monitoring requirements. The instrument, based on direct laser absorption spectroscopy in the mid-infrared region (near 6.01 µm), leverages on recent advances in laser sources and laser driving concepts, and has been extensively characterized in laboratory experiments under UTLS-relevant conditions (Brunamonti et al., 2023; 2025). With a total weight of 3.6 kg, ALBATROSS is compatible with routine deployment on lightweight meteorological balloons.

In this study, we present the in-flight validation of ALBATROSS, based on seven balloon flights conducted between 2022 and 2026 from the meteorological observatories of Payerne, Switzerland (six flights) and Lindenberg, Germany (one flight). The Payerne campaigns were carried out in the framework of the GAW/GCOS-CH project "Swiss H_2O Hub", featuring a comprehensive suite of co-located in situ and remote-sensing instruments. All flights included simultaneous measurements by a CFH hygrometer and a standard meteorological radiosonde. Instrument configuration and payload integration are described in Sections 2 and 3, respectively. The results are presented in Section 4 and discussed in Section 5.

2. Instrument description

The balloon-borne laser absorption spectrometer for UTLS water research, ALBATROSS, has been described in detail elsewhere (Graf et al., 2021). Here, we summarize the instrument architecture and highlight the specific design elements relevant for its operation under UTLS flight conditions.

https://doi.org/10.5194/egusphere-2026-4762
Preprint. Discussion started: 25 August 2026

2.1. Main components

ALBATROSS uses a quantum-cascade laser (QCL) in combination with a compact, monolithic segmented circular multipass cell (SC-MPC; Graf et al., 2018). The SC-MPC provides an optical path length (OPL) of 6 m within a 10.8 cm diameter cell, is highly resistant to thermal and mechanical stress (Tuzson et al., 2020), and allows both closed-path (laboratory, e.g.: Brunamonti et al., 2023; 2025) and open-path (flight) operation. A distributed-feedback quantum cascade laser (DFB-QCL; Alpes Lasers, Switzerland), tuned over a spectral window of ~1 cm^{-1} centred around an isolated absorption line of H_2O at 1662.809 cm^{-1}, is used as a light source. Rapid spectral sweeping is achieved using the intermittent continuous wave (iCW) driving approach (Fischer et al., 2014), implemented via custom analog electronics (Liu et al., 2018). The transmitted laser radiation is detected using a thermoelectrically cooled MCT detector (Vigo Photonics, Poland). Signal acquisition and preprocessing are handled by an FPGA-based system-on-chip (Red Pitaya, Slovenia). Spectra are acquired at 3 kHz and co-averaged to a temporal resolution of 1 Hz. Thermal control and stabilization of the optoelectronic components is achieved by a combination of thermoelectric cooling and passive temperature buffering (Graf et al., 2021). All data are stored locally on a USB drive and retrieved after payload recovery.

For the balloon flights, ALBATROSS is operated in an open-path configuration, allowing ambient air to freely stream through the central intake tube and the SC-MPC during ascent and descent (see Fig. 1). The instrument is integrated into a lightweight enclosure built from carbon-aramid honeycomb plates with a thickness of 4 mm and external dimensions of 31×23×12 cm^3. This enclosure replaces the heavier PMMA box used in earlier deployments (Graf et al., 2021), significantly reducing the overall payload mass. On both sides of the SC-MPC, the cell is connected via nitrile O-rings to an aluminium "funnel", coated with an inert surface treatment (SilcoNert, USA). This funnel is extended over the enclosure by about 12 cm by two thin-walled stainless-steel intake tubes (wall thickness 0.05 mm, inner diameter 8 cm). This design replaces the PTFE-inlet duct of the original configuration and is critical for minimizing self-contamination effects from moist air within the instrument's enclosure (see below). Temperature, pressure and relative humidity (RH) inside the enclosure are monitored during flight by a compact sensor (MS8607; TE Connectivity, USA).

ALBATROSS operates autonomously for the duration of a typical balloon flight (2–3 h). It has a power consumption of about 15 W, which is provided by two 4-cell Lithium-Polymer (LiPo) batteries (14.8 V; 1800 mAh). The weight of the bare spectrometer assembly (as shown in Fig. 1b), including batteries, is 2.91 kg. For flight operation, the instrument is enclosed in a 3 cm thick extruded polystyrene foam (XPS) insulation layer (weight 370 g). In addition, an external in-flight purging system (described below) is added, with a weight of 320 g, yielding a total mass of 3.6 kg.

The spectrometer has been extensively characterized in laboratory experiments under UTLS-relevant conditions (Brunamonti et al., 2023; 2025). These studies demonstrated an accuracy better than ±1.5 % with respect to an SI-traceable reference for H_2O mixing ratios between 2.5 and 35 ppm at pressures of 30–250 hPa and a precision better than 30 ppb at 1 s time resolution (Brunamonti et al., 2023). In the AquaVIT-4 intercomparison, ALBATROSS showed good performance across a dynamic range of 0.5–530 ppm H_2O and a wide range of challenging environmental conditions, achieving a mean deviation of 3 ± 9 %

https://doi.org/10.5194/egusphere-2026-4762
Preprint. Discussion started: 25 August 2026

relative to a reference dewpoint mirror hygrometer (Brunamonti et al., 2025). Despite this comprehensive laboratory characterization, ALBATROSS has not yet been systematically validated under real UTLS conditions and in direct comparison with established balloon-borne reference instruments.

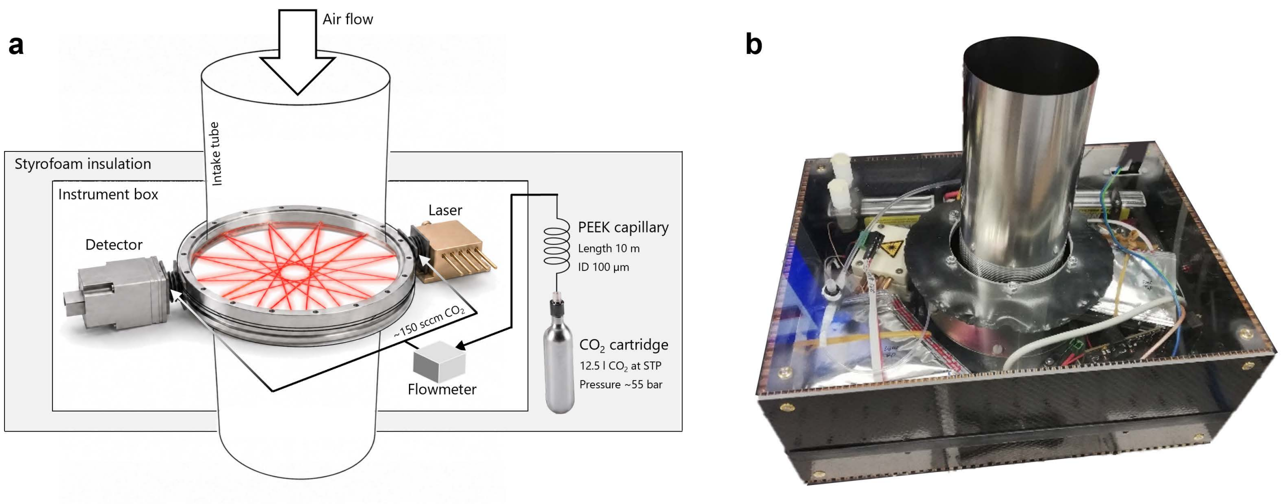

Figure 1. Panel (a): schematics of the ALBATROSS payload, illustrating the purge gas release system for minimizing internal contamination. Panel (b): picture of ALBATROSS spectrometer in flight configuration (without purge system).

2.2. Technical challenges

The first balloon test flight of ALBATROSS, performed in 2019 (Graf et al., 2021), demonstrated a reliable instrument performance up to an altitude of about 10 km. At higher altitudes, however, the retrieved H_2O mixing ratio exhibited a pronounced moist bias, increasing with altitude and reaching values up to ~100 ppm. This bias was traced back to contamination by water vapor desorbing from internal surfaces of the instrument enclosure during flight.

The amount of moisture contained in the enclosure is largely determined by the H_2O trapped inside the instrument at launch and its subsequent release during ascent. At decreasing ambient pressure, desorption of H_2O from internal surfaces is enhanced, and the comparatively warm temperature inside the enclosure allows the released H_2O to remain in the gas phase. Housekeeping data from the embedded RH sensor show that temperature in the enclosure remains at about –10 °C throughout the stratosphere, while internal RH reaches about 20 % at 30 km altitude (see Fig. S3 in Supplementary material). This corresponds to an H_2O mixing ratio of about 5×10^4 ppm inside the enclosure, several orders of magnitude higher than ambient UTLS air (a few ppm). Due to this extremely large gradient, even small absorption contributions from air inside the enclosure can introduce significant retrieval biases. In the following, the dominant contamination pathways are discussed.

Outside-cell absorption. One major contamination pathway arises from outside-cell absorption, i.e., absorption of laser radiation by water vapor along the short free optical path between the optoelectronic components (laser and detector) and the

https://doi.org/10.5194/egusphere-2026-4762
Preprint. Discussion started: 25 August 2026

SC-MPC. As discussed in Graf et al. (2021), these highly temperature-sensitive components cannot be placed in direct thermal contact with the SC-MPC, which is fully exposed to the ambient air temperature variations. Although this internal path represents only ~0.1% of the total OPL, absorption by H_2O present in the enclosure can introduce a substantial bias in the retrieved mixing ratios under UTLS conditions. This effect becomes particularly pronounced at high altitudes, where low pressure enhances desorption of H_2O from internal surfaces.

To eliminate this interference, a mechanical solution was implemented in the form of two custom-made connectors that hermetically connect the detector and the laser housing to the SC-MPC, thereby isolating the free optical path from the humid air inside the enclosure. The connectors are 3D-printed and provide sufficient mechanical flexibility for optical alignment while maintaining thermal decoupling between the components and the cell. In addition, the connectors incorporate a gas port that allows active purging with dry gas and maintaining a slight overpressure relative to the enclosure. Laboratory experiments demonstrated that purging with N_2 at a flow rate of 0.1 slpm effectively suppresses any spurious absorption originating from outside-cell paths (Brunamonti et al., 2023; 2025).

For balloon operation, this concept was further developed into a lightweight in-flight purging system, capable of maintaining dry conditions within the connectors throughout the duration of a balloon sounding. This system uses a commercially available miniature CO_2 cartridge (containing 25 g of CO_2) as a compact source of dry gas compatible with balloon operation. A custom release valve combined with a passive flow restriction limits the purge flow rate to roughly 0.1 slpm, resulting in a slow release lasting about 3 hours. The flow restriction consists of a PEEK capillary tubing with length of 10 m and inner diameter ~100 µm (TPK104; VICI, USA). In addition, a chip-size flowmeter (Omron, USA) was integrated to monitor the purge gas delivery during flight and provide diagnostic information for the interpretation of the measured data.

During some flights, interruptions of the purge gas flow, caused by clogging due to the formation of dry ice (solid CO_2) at low temperatures were observed. This issue was attributed to excessive cooling of CO_2 during the free expansion (Joule–Thomson effect) within the capillary. Iterative thermal management improvements were implemented, including the addition of heating elements to both the CO_2 cartridge and, critically, the PEEK capillary. The specific configuration of the purging system used in individual flights and their impact on the measurement performance are discussed in Section 4.1.

In-cell contamination. A second contamination pathway arises when moisture from the instrument enclosure enters the multipass cell. Since the H_2O mixing ratio inside the enclosure (10^4–10^5 ppm) exceeds typical stratospheric conditions (a few ppm) by several orders of magnitude, even tiny leakages can introduce substantial retrieval biases. Early flights revealed that the original mechanical interface between the enclosure and the SC-MPC was insufficiently leak-tight, leading to a positive bias and high-frequency fluctuations in the stratospheric H_2O retrievals. To suppress this effect, the interface was redesigned using custom 3D-printed adapters with nitrile O-ring seals, improving leak tightness while preserving mechanical isolation of the optical system. The effectiveness of this solution is demonstrated by the flight results presented in Section 4.

External moisture sources. Contamination effects induced by external moisture sources are common to balloon-borne hygrometers and can affect all in situ measurements in the stratosphere. These include sublimation of hydrometeors potentially collected by the intake tube during cloud passage (e.g., Brunamonti et al., 2018; Jorge et al., 2021), as well as desorption of

https://doi.org/10.5194/egusphere-2026-4762
Preprint. Discussion started: 25 August 2026

H_2O molecules from components of the balloon train, such as string, parachute, and balloon envelope (Hall et al., 2016; Vömel et al., 2016). The impact of these effects ranges from severe contamination of the entire stratospheric profile due to sublimation after passing through mixed-phase clouds (Jorge et al., 2021), to small transient enhancements in H_2O caused by passage of the payload through the moist wake of the balloon. These short-duration perturbations, commonly referred to as "balloon spikes", are routinely observed in CFH soundings (e.g., Vömel et al., 2007). In this study, balloon spikes are explored as a naturally occurring impulse-response experiment to evaluate the dynamic response of the instruments (Section 4.3).

3. Measurements overview

Between 2022 and 2026, a total of seven flights were performed to validate the performance of ALBATROSS (see Table 1). The first test flight (F0) took place in September 2022 from the Lindenberg Meteorological Observatory (Germany), operated by the Deutscher Wetterdienst (DWD). Subsequently, six flights were performed between August 2023 and May 2026 from the aerological station of MeteoSwiss at Payerne (Switzerland), within the framework of the GAW/GCOS-CH project "Swiss H_2O Hub". This project aims at providing vertically resolved observation of atmospheric water vapor from the ground to the middle atmosphere through the coordinated operation of complementary in situ and remote-sensing techniques. While several additional instruments were operated during these campaigns, the present study focuses exclusively on the balloon-borne in situ measurements relevant for the validation of ALBATROSS.

Each balloon payload included the ALBATROSS spectrometer and an RS41 radiosonde (Vaisala, Finland), providing pressure (p) temperature (T), relative humidity (RH) and GPS position data at 1 s resolution (Vaisala, 2024). In addition, a CFH hygrometer was used as a reference instrument for UTLS H_2O. In the first four flights (F0-F3), payload mass restrictions required ALBATROSS and CFH to be flown on separate balloons, with launch times separated by less than one minute (i.e., "tandem" flight configuration). From flight F4 onwards, following approval by the Swiss civil aviation authority (BAZL), ALBATROSS and CFH were integrated on the same balloon (total payload weight ~6 kg). The impact of the flight configuration and related atmospheric variability effects on the quality of the intercomparison is discussed in Section 4.

All flights were carried out using 2000–3000 g latex balloons (TOTEX, Japan), providing a ceiling altitude of up to 35 km with an ascent rate of approximately 5–6 m s^{-1} (see Fig. 2). The scientific payload was attached to the balloon through a swivel and a 60 m unwinder (GRAW, Germany) to minimize contamination from the balloon surface. Above the unwinder, a parachute (Spekon, Germany) and a cut-down system (Loonatec, USA) were installed to control the ceiling altitude. In accordance with civil aviation requirements, a lightweight transponder (uAvionix, USA) was included to ensure visibility to air traffic control. An independent GPS tracker (Twig, Finland) was used to facilitate payload recovery. All launches were performed at nighttime (22–03 LT), although ALBATROSS can also be operated during daytime.

The Vaisala RS41 is a high-quality meteorological radiosonde, widely used in operational observational networks. Relative humidity measurements are based on the thin-film capacitor technique (Survo et al., 2014) with a manufacturer-specified RH resolution of 0.1 % and a combined uncertainty of 4 % (Vaisala, 2024). Although, under given conditions, RS41 can provide

https://doi.org/10.5194/egusphere-2026-4762
Preprint. Discussion started: 25 August 2026

reliable measurements for a few km above the tropopause (Brunamonti et al., 2019), here we choose for consistency to only retain tropospheric data by RS41 for the statistical comparison (see Section 4). RH measurements from RS41 are converted to H_2O mixing ratio using the Hardy (1998) formulation of the Wexler (1976) parameterization for saturation vapor pressure over liquid water (recommended for Vaisala data products: see Brunamonti et al., 2019).

CFH is a long-standing reference instrument for balloon-borne measurements of UTLS H_2O within GRUAN and NDACC. Under stable operating conditions, CFH uncertainties can be as low as 2–4 % in the UTLS, corresponding to ~0.2 K uncertainty in frostpoint temperature (Vömel et al., 2016). Rapid changes in environmental conditions during balloon ascent, however, can introduce nonequilibrium effects associated with the response time of the mirror temperature controller, leading to transient errors that may exceed ±10 % in mixing ratio (Poltera et al., 2026). In this work, regions showing large nonequilibrium fluctuations are discarded, and residual errors are mitigated by applying a broad altitude averaging (250–500 m) in the statistical comparison (Section 4). Frostpoint temperature measurements by CFH are converted to H_2O mixing ratio using pressure from RS41 and the parameterization for saturation vapor pressure over ice by Murphy and Koop (2005). All flights considered here employed freon R23 (i.e., trifluoromethane) as a cooling agent for CFH, except F2 in which a refrigerant mixture based on dry ice and alcohol was used (tested as part of the Swiss H_2O Hub project activities).

Since ALBATROSS is a prototype instrument, payload recovery after each flight was essential, imposing strict constraints on launch conditions. Soundings were scheduled only when trajectory forecast indicated a high probability of recovery in accessible terrain, and when meteorological conditions were free of precipitation and low and/or mid-level cloud layers at launch time. The latter criterion is particularly important to avoid contamination by supercooled liquid droplets, which can freeze on instrument inlets and subsequently evaporate at stratospheric altitudes (Jorge et al., 2021). Flight planning was supported by a combination of weather forecasting tools, including operational systems available at MeteoSwiss, and Lagrangian trajectory models (Sprenger and Wernli, 2015) driven by forecast data from the European Centre for Medium-Range Weather Forecasts (ECMFW), enabling reliable prediction of the balloon trajectories and landing locations.

ID	Date, Time	Station	Payload balloon 1	Payload balloon 2	Ceiling altitude
F0	2022-09-17, 03 LT	Lindenberg	ALBATROSS, RS41	CFH, RS41	30 km
F1	2023-08-17, 23 LT	Payerne	ALBATROSS, RS41	CFH, RS41	28 km
F2	2024-06-18, 22 LT	Payerne	ALBATROSS, RS41	CFH, RS41	15 km
F3	2024-09-19, 03 LT	Payerne	ALBATROSS, RS41	CFH, RS41	35 km
F4	2025-03-27, 23 LT	Payerne	ALBATROSS, CFH, RS41	-	25 km
F5	2025-07-01, 00 LT	Payerne	ALBATROSS, CFH, RS41	-	27 km
F6	2026-05-01, 00 LT	Payerne	ALBATROSS, CFH, RS41	-	28 km

Table 1. List of all balloon flights performed with ALBATROSS between 2022 and 2026.

https://doi.org/10.5194/egusphere-2026-4762
Preprint. Discussion started: 25 August 2026

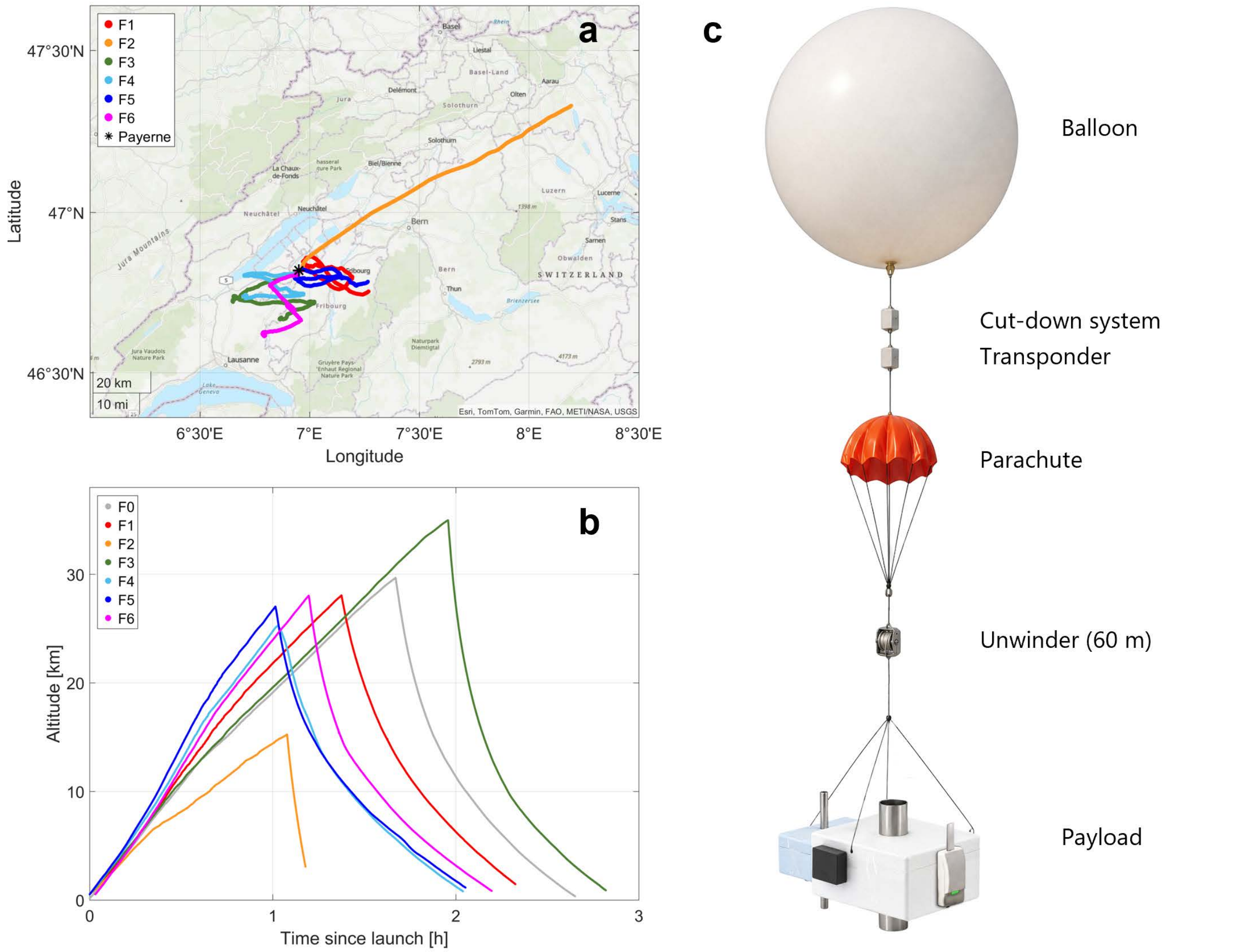

Figure 2. Panel (a): trajectories of balloon flights F1-F6 performed from Payerne (map sources: Esri, TomTom, Garmin, FAO, METI/NASA, USGS | Powered by Esri); (b): altitude vs. time profiles of all balloon flights (F0-F6); (c): schematics of balloon train assembly with ALBATROSS and CFH on the same payload (flights F4-F6).

4. Results

Figure 3 shows the vertical profiles of H_2O mixing ratio measured by ALBATROSS, CFH and RS41 during the ascent of all flights (panels a-g) and the descent of F6 (panel h), at 1 s temporal resolution. Dark-coloured dots denote valid data, while light-coloured dots indicate flagged measurements, i.e., data points which are considered invalid and thus are excluded from the statistical comparison. The descent of flights F0-F5 is shown in Figure S1 in Supplementary material.

ALBATROSS data are flagged based on characteristic signatures associated with the contamination mechanisms introduced in Section 2.2, such as interruptions of the purge gas flow measured by the embedded flowmeter (outside-cell absorption), and

https://doi.org/10.5194/egusphere-2026-4762
Preprint. Discussion started: 25 August 2026

a conservative filter applied when no suitable diagnostics information are available (in-cell contamination, external moisture sources). The performance of ALBATROSS and related contamination issues are discussed flight-by-flight in the next section. CFH profiles were individually quality-checked and flagged for contamination by external moisture sources, nonequilibrium errors, and other technical failures, as discussed in Section S2 in Supplementary material. RS41 measurements are considered valid in the troposphere and flagged above the tropopause. Note that a list of all ALBATROSS and CFH flagged data intervals and their corresponding rationale can be found in Table 1 in Supplementary material.

ALBATROSS underwent iterative hardware modifications throughout the validation campaign, in response to the findings of each flight. Therefore, individual soundings reflect progressively improved configurations of the instrument. In the following, the results are first summarized in chronological order to document the evolution of the instrument's performance. Then, tropospheric and stratospheric measurements are discussed in detail in Sections 4.2 and 4.3, respectively, followed by a statistical evaluation of all flights in Section 4.4.

4.1. Flight-by-flight performance summary

Flight F0 was performed with an early version of the in-flight purging system, using a stainless-steel critical orifice as a flow restriction and no flowmeter. While the data showed good agreement with CFH and RS41 in the troposphere (below ~12 km), the stratospheric retrieval was affected by a substantial moist bias (up to 200 ppm, increasing with altitude) and high-frequency fluctuations (peak-to-peak ~50 ppm, frequency 5−10 s). Spectral analysis confirmed that this behaviour did not originate from the spectroscopic retrieval, but rather from contamination by an external H_2O source. In the absence of flowmeter diagnostics, this was attributed to a combination of outside-cell absorption and in-cell contamination mechanisms.

Flight F1 employed a revised purging configuration, including PEEK capillary and flowmeter. Despite this upgrade, the stratospheric data still exhibited a pronounced moist bias similar to F0. The flowmeter data revealed that the purge gas was correctly delivered (flow rate ≥ 0.1 slpm) up to ~21 km altitude (50 hPa), while it ceased abruptly at this level, coinciding with a clear increase in the observed rate of contamination (see Fig. 3b). Therefore, the bias in ALBATROSS below 21 km was attributed to in-cell contamination, motivating a redesign of the intake system, as described in Section 2.2.

Flight F2 was terminated at ~15 km altitude (120 hPa) by cut-down release due to geofencing constraints imposed by BAZL. The large horizontal drift of the balloon in this flight (see Fig. 2a) was caused by an anomalously low ascent rate (Fig. 2b), possibly due to enhanced drag effects by the parachute in a strong wind field. Despite the reduced ceiling altitude, the ALBATROSS data shows good agreement with CFH and RS41 up to 15 km, and no evidence of contamination or fluctuations in the stratosphere. This result demonstrated that the revised intake tube design and regular operation of the in-flight purging system effectively suppress both outside-cell and in-cell contamination and marked the first successful measurements of ALBATROSS in the stratosphere, with ~4 km of high-quality data above the tropopause.

Flight F3 reached an altitude of 35 km (~6 mbar) and was carried out using the same configuration as F2. The overall agreement between ALBATROSS and CFH was good across the entire profile, although a few instances of increase in the retrieved

https://doi.org/10.5194/egusphere-2026-4762
Preprint. Discussion started: 25 August 2026

H_2O were observed in the stratosphere (flagged data points in Fig. 3d). These were found to correlate with interruptions in the purge gas flow measured by the embedded flowmeter (see Fig. S3 in Supplementary material), and attributed to the clogging of the purging system caused by dry ice formation in the release system. Using the flowmeter diagnostics, these contamination events can be modelled by a diffusion model, allowing partial correction of the affected data (discussed in detail in Sections 4 and S2). Note that in this flight, the CFH profile was affected by large instrumental fluctuations (nonequilibrium errors) up to ~70 hPa ascent, which were smoothed by a moving average (see Section S1 in Supplementary material).

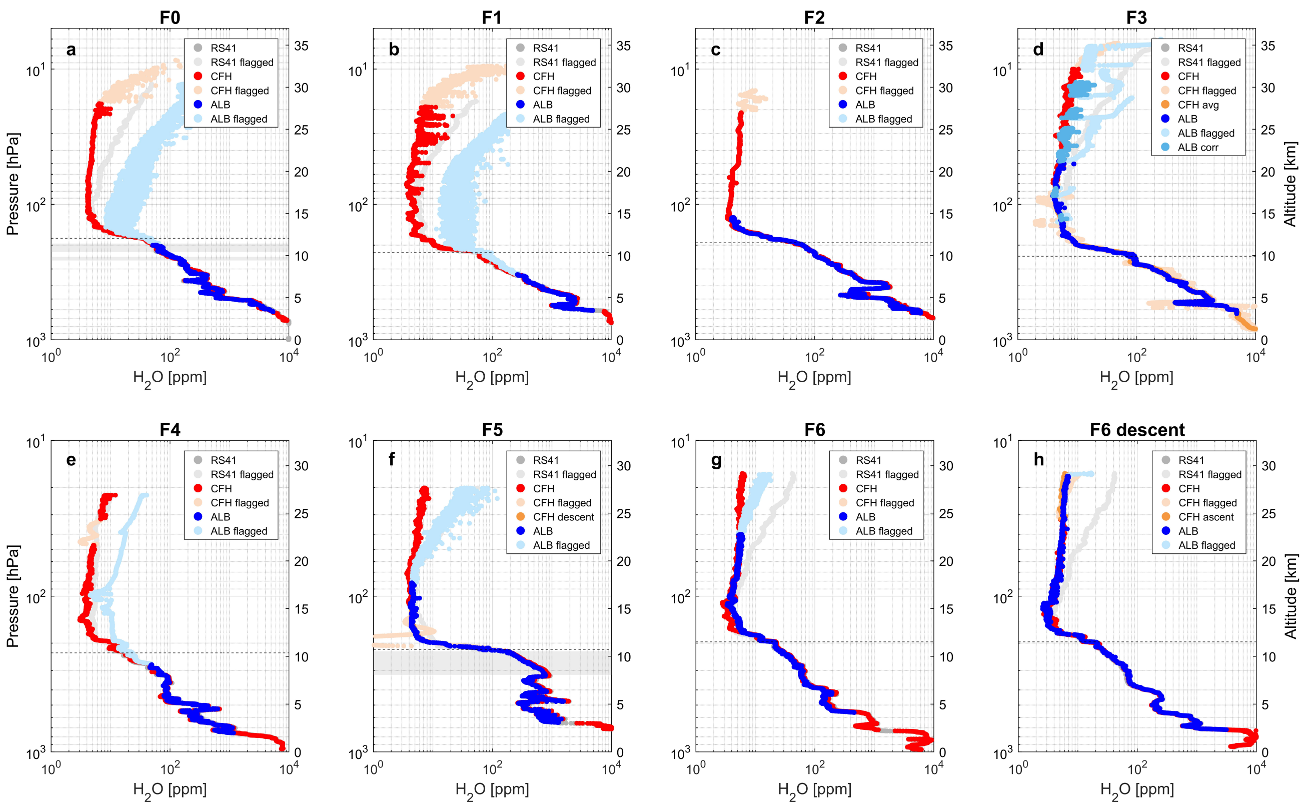

Figure 3. Vertical profiles of H_2O mixing ratio as a function of pressure measured by ALBATROSS (blue), CFH (red) and RS41 (grey) during the ascent of all flights at 1 s resolution. Light-colored and dark-colored dots indicate flagged and valid data points, respectively. Black dashed horizontal lines indicate the level of the tropopause. Grey shadings in panels a and f indicate the layers of cirrus clouds, inferred from CFH ice saturation measurements. Turquoise dots in panel d (F3) indicate ALBATROSS measurements corrected by a diffusion model (see Sections 4 and S2). Orange dots in panels d, f and h indicate CFH measurements smoothed by a moving average (F3) and replaced by descent (F5) or ascent (F6) profiles (see Section S1 in Supplementary material).

https://doi.org/10.5194/egusphere-2026-4762
Preprint. Discussion started: 25 August 2026

Flight F4 was the first co-located flight of ALBATROSS and CFH. Despite the application of a heating element to the CO_2 cartridge to prevent clogging of the release system, the purge gas delivery failed at ~10 km altitude during ascent. Nevertheless, the data are still valuable and enable a direct comparison between the two instruments in the troposphere. In addition, two pronounced "balloon spikes", observed simultaneously by ALBATROSS and CFH at ~23 km altitude, provide a unique opportunity to compare the dynamic response of the two instruments in the stratosphere (Section 4.3).

Flight F5 employed an optimized purging configuration with active heating applied to both CO_2 cartridge and the capillary, targeting clogging caused by cooling during gas expansion by Joule-Thomson effect. This effect can account for a gas cooling by as much as ~67 K with a pressure difference of 56 bar between inlet (~57 bar, saturation vapor pressure of CO_2 at 23 °C) and outlet (≤ 1 bar) of the capillary, based on literature values (Wang et al., 2017). Under this configuration, the purge flow remained constant at 0.1–0.15 slpm throughout the entire flight. Yet, the stratospheric data still show evidence of contamination above 60 hPa, increasing with altitude (Fig. 3f). This was attributed to external moisture sources, and particularly a thick cirrus cloud crossed by the balloon in the upper troposphere (~9–11 km altitude), likely containing supercooled water droplets (cloud bottom temperature around –32°C), which are known as a severe source of contamination (Jorge et al., 2021).

Flight F6 was carried out with the same configuration as F5 and was characterized by an excellent agreement between ALBATROSS and CFH throughout the entire profile, both in ascent (Fig. 3g) and descent (Fig. 3h) data. The ascent profile still shows evidence of residual contamination above 40 hPa pressure (~23 km altitude), which was attributed to external contamination by the strings, parachute or balloon envelope. In contrast, the descent data shows a close agreement with CFH at all levels, from the lower troposphere (~2 km altitude), with > 5000 ppm H_2O content, to the lower stratosphere (~28 km altitude), with 4–6 ppm H_2O, including a particularly dry tropopause region (~3 ppm H_2O at 150 hPa).

4.2. Troposphere

Figure 4 presents a detailed comparison of the H_2O mixing ratio profiles measured by ALBATROSS, CFH, and RS41 in the troposphere, covering pressures between 200 and 800 hPa (corresponding to ~2–12 km altitude), during the ascent of all flights (panels a-g). Vertical profiles of the relative difference (ΔH_2O) between ALBATROSS and RS41 (blue) and ALBATROSS and CFH (red) in the same altitude range are shown in panels h-n.

The differences are calculated in altitude (z) bins of 250 m width for $z < 12$ km (i.e., troposphere) and 500 m for $z > 12$ km (stratosphere), based on GPS altitude measured by the RS41 radiosonde. This averaging interval was chosen to minimize errors due to atmospheric variability and nonequilibrium states of CFH. Error bars represent the mean ± standard deviation (σ) range of ΔH_2O in each bin. Note that the ALBATROSS retrieval typically starts between 2 and 4 km altitude, as the spectral window becomes saturated at the high H_2O mixing ratios encountered close to the surface (see Graf et al., 2021).

Across all flights, ALBATROSS shows a generally good agreement with both CFH and RS41 in the troposphere, with mean deviations predominantly within ±10 % relative to both reference instruments. This level of agreement is maintained over a dynamic range spanning nearly three orders of magnitude in H_2O mixing ratio, down to values well below 100 ppm (F3, F6).

https://doi.org/10.5194/egusphere-2026-4762
Preprint. Discussion started: 25 August 2026

The only notable exceptions occur in the upper troposphere of flights F1 (Fig. 2i) and F4 (Fig. 2l), where the onset of contamination at ~8–9 km leads to larger deviations. In all other flights, the agreement extends to at least the local tropopause (11–12 km). The ALBATROSS profiles closely reproduce vertical fine structures in the distribution of H_2O, demonstrating the capability of the laser absorption technique to resolve sharp gradients and mesoscale variability. Notably, good performance is maintained within and below cirrus cloud layers, as illustrated by flights F0 and F5, indicating that ALBATROSS measurements are not adversely affected by the presence of ice clouds in the troposphere.

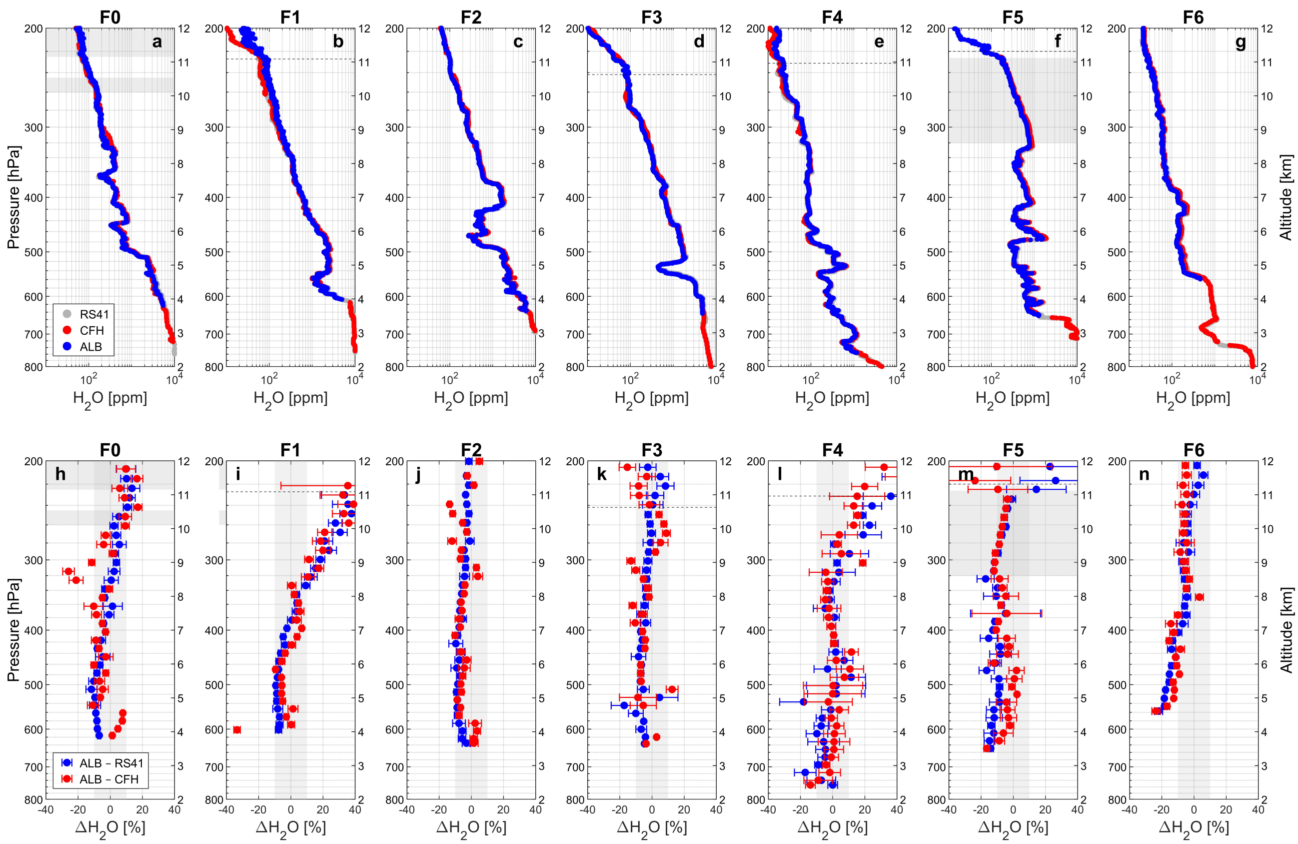

Figure 4. Panels (a-g): vertical profiles of H_2O mixing ratio measured by ALBATROSS (blue), CFH (red) and RS41 (grey) during the ascent of all flights, at 1 s resolution, for the tropospheric region (200−800 hPa pressure, ~2−12 km altitude). Panels (h-n): mean ± standard deviation (σ) profiles of the relative differences (ΔH_2O) of ALBATROSS – RS41 (blue) and ALBATROSS – CFH (red), calculated in bins of 250 m (500 m) for z < 12 km (z > 12 km) for all data points (including flagged measurements). Black dashed horizontal lines indicate the level of the tropopause and horizontal grey shaded areas indicate cirrus cloud layers. In panels (h-n), the vertical grey shading indicates a deviation range of ±10 %. Note that the altitude scale on the right-hand side is approximated and does not represent the GPS altitude measured by RS41.

https://doi.org/10.5194/egusphere-2026-4762
Preprint. Discussion started: 25 August 2026

A substantial distinction between the RS41 and CFH comparisons consists in the fact that RS41 was flown on the same balloon as ALBATROSS in all flights, whereas the CFH comparison is based on a combination of tandem (i.e., separate balloons: F0–F3) and co-located (F4–F6) flights (see Section 3). Given the typically low spatial and temporal variability of UTLS H_2O, the tandem flight configuration generally allows for a meaningful comparison of the two instruments, as shown in Fig. 4. However, small differences in ascent rate can lead to significant horizontal and vertical separation between the two balloons in the upper troposphere, which can cause discrepancies due to atmospheric variability effects. Although these effects are largely mitigated by the broad altitude averaging used here, this might explain the larger deviations found in ALBATROSS – CFH compared to ALBATROSS – RS41 in the upper troposphere (~8–12 km altitude) of flights F2-F3 (Fig. 4j-k).

An additional advantage of the co-located flight configuration is to enable a direct comparison between ALBATROSS and CFH during both the ascent and descent phase of the soundings. Fig. 5 demonstrates the good agreement achieved by ALBATROSS with respect to CFH in the descent of co-located flights F4 and F6, including a remarkable performance in flight F6 with mean deviations from CFH better than ±5 % at all altitudes (Fig. 5d).

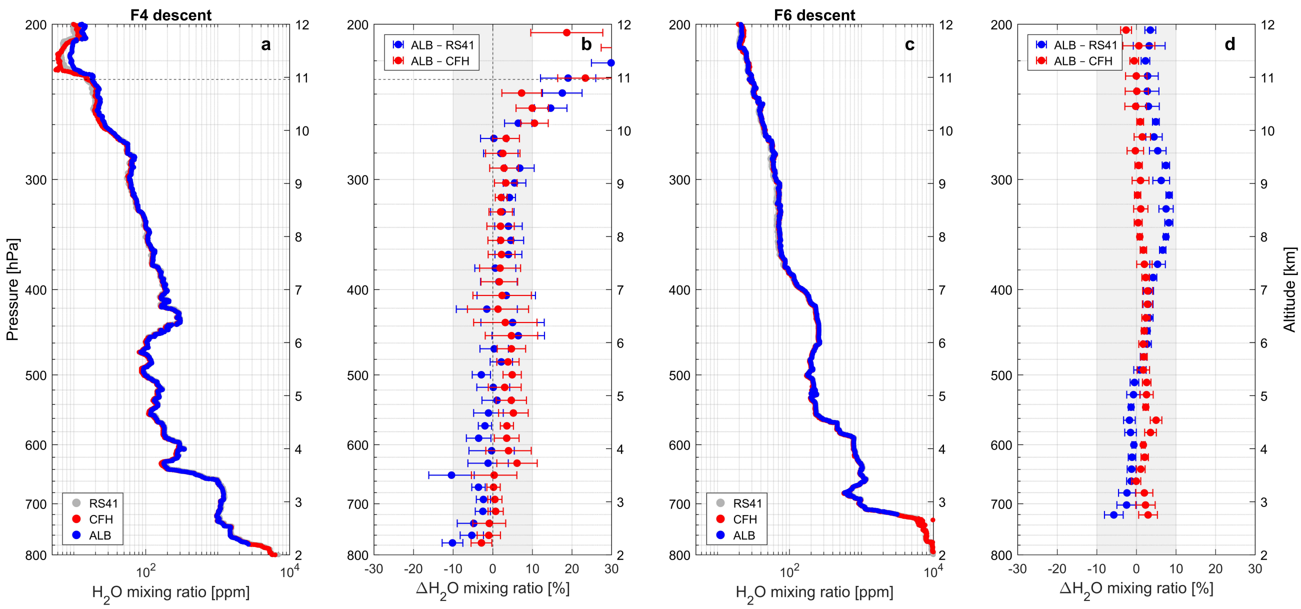

Figure 5. Panels (a, c): vertical profiles of H_2O mixing ratio measured by ALBATROSS (blue), CFH (red) and RS41 (grey) during the descent of flights F4 (a) and F6 (c) at 1 s resolution in the troposphere (200−800 hPa pressure, ~2−12 km altitude). Panels (b, d): vertical profiles of the relative differences (ΔH_2O) of ALBATROSS – RS41 (blue) and ALBATROSS – CFH (red) in the same region of F4 (panel b) and F6 (d), for all data points (including flagged measurements). Horizontal black dashed lines indicates the tropopause level. The grey shading in panels (b, d) indicates a deviation range of ±10 %.

https://doi.org/10.5194/egusphere-2026-4762
Preprint. Discussion started: 25 August 2026

4.3. Stratosphere

Due to the contamination issues discussed above, valid ALBATROSS measurements above the tropopause were obtained in four out of seven validation flights: F2, F3, F5 and F6 (both ascent and descent) (see Fig. 3). In addition, flight F4, although affected by overall contamination, provides valuable information on the temporal response of ALBATROSS in comparison with CFH. In this section, we focus on the stratospheric analysis of flights F3, F4 and F6, which together allow an assessment of both measurement accuracy and dynamic response.

Figure 6 shows the profiles of H_2O mixing ratio measured by ALBATROSS and CFH in the stratosphere (5–250 hPa pressure, ~10–36 km altitude) during the ascent of flight F3 (panel a) and the descent of flight F6 (panel b).

During F3, the ALBATROSS retrieval exhibited alternating intervals of good agreement with CFH and short periods affected by contamination (see Fig. 3d), which were found to coincide with interruptions in the purge gas flow. Particularly, the analysis of the flowmeter data (shown in Fig. S2 in Supplementary material) reveals that when the purge gas is supplied continuously, ALBATROSS and CFH agree closely down to ~4 ppm (e.g., around 100 hPa). In contrast, when the purge flow drops to zero, the ALBATROSS retrieval shows a characteristic exponential increase in H_2O. Assuming that this process is governed by the diffusion of moist air from the instrument's casing into the connector's volume, leading to outside-cell absorption (see Section 2.2), the affected regions of the ALBATROSS retrieval can be partially modelled and corrected using an exponential function. The complete correction procedure is described in detail in Supplementary material (Section S2), and the resulting corrected data points are shown in Fig. 6a as turquoise dots. An independent consistency check of this approach, based on the measured H_2O mixing ratio inside the instrument's enclosure derived from housekeeping data, is also provided in Section S2 (Fig. S3), lending confidence to the physical interpretation of the contamination mechanism.

After this correction, ALBATROSS and CFH agree within ±10 % up to ~24 km altitude (30 hPa) (Fig 6a). This includes the region between 45–120 hPa (~12–22 km altitude), encompassing the hygropause (~4 ppm at 90 hPa), during which the purge gas supply was largely uninterrupted (Fig. S2). Above ~24 km altitude, ALBATROSS shows a slight moist bias of 1–2 ppm relative to CFH, attributed to external moisture sources. During descent, the entire stratospheric profile of F3 was contaminated, as the purge gas delivery terminated shortly before the balloon burst (see Fig. S2).

The descent of flight F6 (Fig. 6b) provides the most complete uncontaminated stratospheric dataset obtained during the validation campaign and thus represents the best assessment of ALBATROSS performance under flight conditions. The measurements show close agreement between ALBATROSS and CFH throughout the entire UTLS, including a particularly dry tropopause with H_2O mixing ratios down to 3 ppm (~14–16 km altitude), and the lower stratosphere with 4–6 ppm up to ~28 km altitude (15 hPa). Across this altitude range, ALBATROSS reproduces the vertical structure observed by CFH while maintaining the low-noise performance demonstrated in laboratory studies. These measurements demonstrate the capability of ALBATROSS to provide high accuracy and high precision measurements of UTLS H_2O up to at least 28 km altitude.

https://doi.org/10.5194/egusphere-2026-4762
Preprint. Discussion started: 25 August 2026

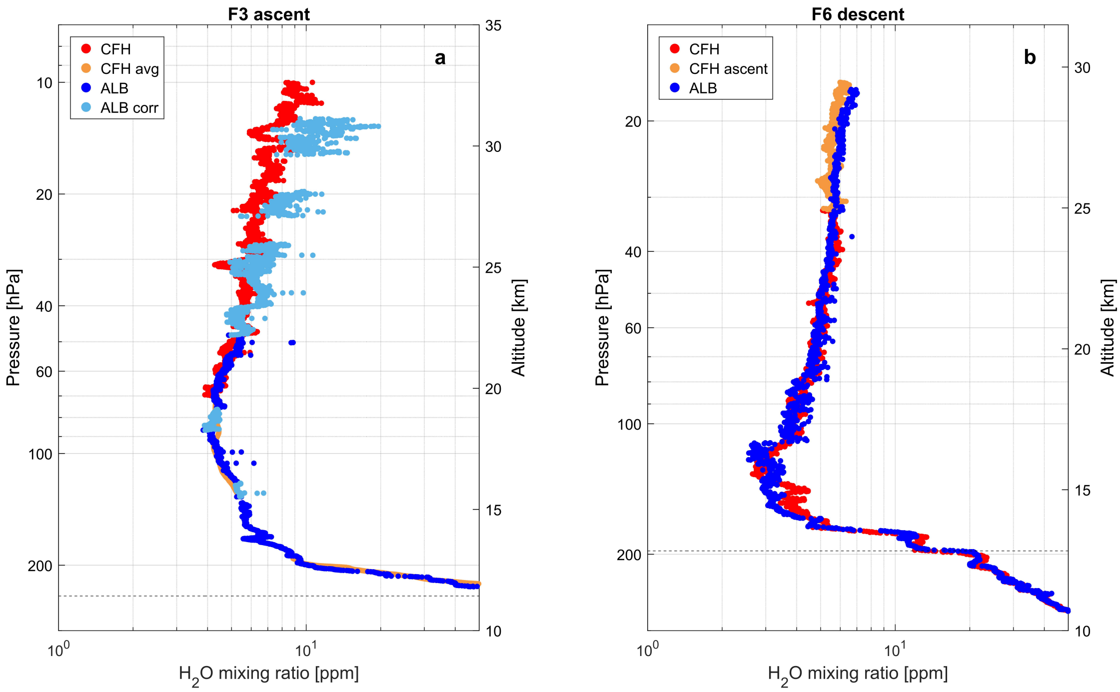

Figure 6. Valid measurements of H_2O mixing ratio as a function of pressure by ALBATROSS (blue) and CFH (red) during the ascent of flight F3 (panel a) and the descent of flight F6 (b) in the stratosphere (5–250 hPa pressure, ~10–36 km altitude). In F3 (panel a), turquoise dots indicate ALBATROSS measurements corrected by a diffusion model (see Section 4). Orange dots indicate CFH measurements smoothed by a moving average (F3, panel a) and replaced by ascent data (F6, panel b) in regions affected by nonequilibrium errors (see Section S1 in Supplementary material). Black dashed lines indicate the level of the tropopause.

A complementary assessment of instrument performance in the stratosphere is provided by so-called balloon spikes observed in flight F4. As introduced in Section 2.2, the term "balloon spike" refers to a small (~1 ppm), transient increase in H_2O due to contamination by H_2O desorption from the balloon skin, when the payload, hanging 60 m below the balloon and following a pendulum-like motion, passes through the wake of the ascending balloon. Such artifacts are used here as a naturally occurring impulse-response experiment to investigate the dynamic response of the instruments.

During F4, two balloon spikes were detected by both ALBATROSS and CFH, flying together in the same payload. Figure 7a-b shows vertical profiles of H_2O mixing ratio measured by CFH, RS41 (panel a) and ALBATROSS (b) between pressures of 28.5–33 hPa (altitude ~22.9–23.8 km) at 1 s resolution during the ascent of flight F4. While the absolute H_2O mixing ratios retrieved by ALBATROSS are affected by contamination of ~15–20 ppm, both instruments clearly record the same transient features at altitudes of about 23.2 km and 23.4 km, confirming their origin as payload-wide contamination events. In contrast, the RS41 shows no evidence of these features, consistent with the slow response and low sensitivity of the thin-film polymer sensor at stratospheric conditions.

https://doi.org/10.5194/egusphere-2026-4762
Preprint. Discussion started: 25 August 2026

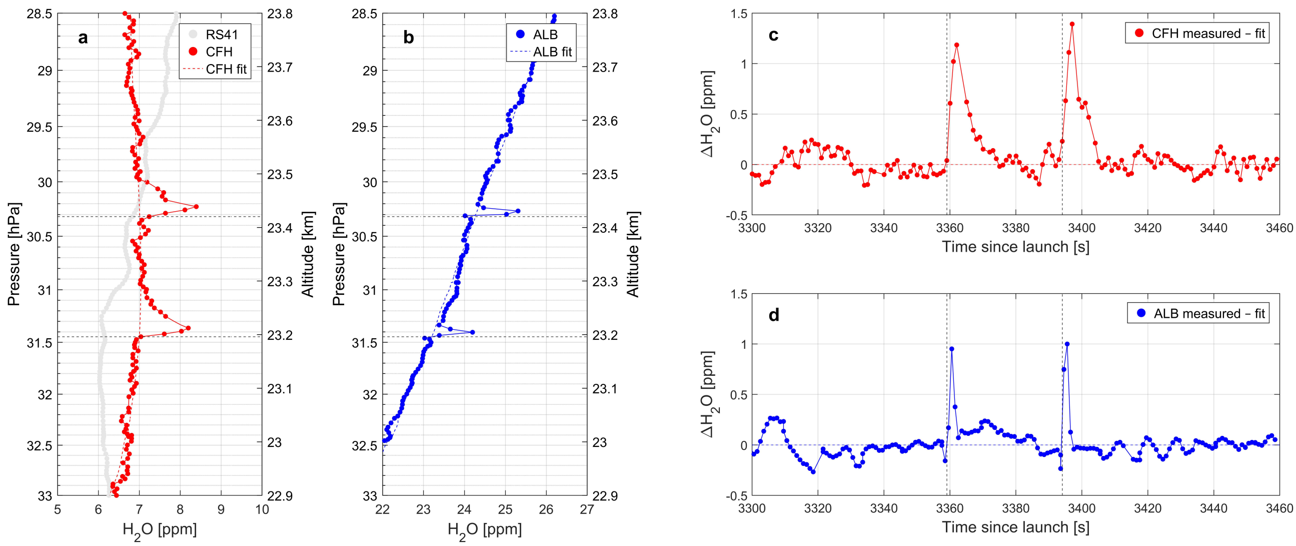

Figure 7. "Balloon spikes" analysis. Panels (a-b): H_2O mixing ratio measured by CFH (red), RS41 (grey) and ALBATROSS (blue) between pressures of 28.5–33 hPa (altitude ~22.9–23.8 km) at 1 s resolution during the ascent of F4. Red and blue dashed lines represent the fitted background profiles for CFH and ALBATROSS, respectively (see Section 4.3) Panels (c-d): timeseries of H_2O mixing ratio by CFH and ALBATROSS over the corresponding time period, after subtracting the background profile. Black dashed lines indicate the onset of the balloon spike perturbations, both in altitude (panels a-b) and time (c-d).

To evaluate the dynamic response of the instruments, Figure 7c-d shows the timeseries of CFH and ALBATROSS over the same time interval, after removal of a smoothly varying background profile. The background was derived by fitting a 2nd order polynomial function to CFH data and a linear function for ALBATROSS data in the vicinity of the spike intervals.
The timeseries show that the perturbation in H_2O lasts about 3 s in ALBATROSS (Fig. 7d), compared to ~10 s for CFH (Fig. 7c) for both spikes. As the data acquisition rate of the laser spectrometer is 1 Hz (involving 3000 spectral averages) and the air exchange within the multipass cell is very short, it is plausible to assume that the duration of the spike in ALBATROSS data corresponds to the passage time of the payload through the wake of the ballon. This is consistent with expected payload motion through the balloon wake, given typical ascent speeds and "swinging" velocities (see Fig. 14 in Jorge et al., 2021). Furthermore, the peak amplitude of the spikes is about 20–40 % higher in CFH (1.2–1.4 ppm) than in ALBATROSS (1 ppm), and the maximum occurs ~2 s later in CFH (Fig. 7c-d). These observations are consistent with an initial overshooting response of the CFH mirror temperature controller, followed by a gradual relaxation towards the baseline value, whereas ALBATROSS captures the perturbation close to its physical duration.
The different relaxation times of the two instruments indicate a substantial difference in their dynamic response, which determines their effective vertical resolution. Assuming that the response time can be estimated by the *e*-folding time (i.e., ~63.2 % relaxation achieved) after the spike perturbation, this corresponds to ~1 s in ALBATROSS (Fig. 7d) and 3–4 s in CFH (Fig.

https://doi.org/10.5194/egusphere-2026-4762
Preprint. Discussion started: 25 August 2026

7c). With an ascent rate of 5–6 m s^{-1}, this corresponds in turn to an effective vertical resolution of 5 m for ALBATROSS and and 15–20 m for CFH. This comparison highlights the advantage of laser spectroscopy over frostpoint hygrometry in terms of temporal response and effective vertical resolution in the stratosphere.

4.4. Statistical comparison

Finally, we present a statistical comparison of ALBATROSS with respect to CFH and RS41 measurements, using data from both the ascent and descent of all flights. Figure 8a-b shows scatter plots of the relative difference in H_2O mixing ratio (ΔH_2O) between ALBATROSS and RS41 (panel a) and between ALBATROSS and CFH (b), as a function of altitude. The differences are calculated in altitude bins of 250 m for $z < 12$ km and 500 m for $z > 12$ km (as in Figs. 4-5). Flagged data points correspond to measurements for which the retrieval of either ALBATROSS, CFH and/or RS41 was flagged. Solid lines represent the mean and the corresponding ± 1 σ standard deviation range of ΔH_2O, averaged over 2 km altitude layers.

Panels c-d show the frequency of occurrence distributions of ΔH_2O for ALBATROSS – CFH (red) and ALBATROSS – RS41 (blue), calculated for all measurements in the stratosphere ($z > 12$ km, panel c) and troposphere ($z < 12$ km, d). The results are summarized in Table 2 in terms of mean ± standard deviation calculated over four atmospherically relevant altitude ranges, including separate estimates of ALBATROSS – CFH for tandem and co-located flights.

Overall, Fig. 8 demonstrates good agreement between ALBATROSS and both reference instruments. In the comparison with RS41, valid data are available up to the tropopause (~12 km altitude), reflecting the loss of sensitivity of the thin-film polymer sensor at stratospheric humidity levels. Within this altitude range, 86 % of the data points fall within deviations of ±10 % (grey shading in Fig. 8a), while the mean profile varies between –5 % and +1 % (Table 2), increasing with altitude. This is largely consistent with the expected uncertainty of RS41 (4 % RH). The few outliers exceeding ±10 % are likely caused by the slow response and time-lag effects of RS41 (e.g. Poltera et al., 2026). Considering all valid tropospheric measurements, the mean ± standard deviation of ALBATROSS – RS41 is –2 ± 7 % (see Table 2).

The comparison with CFH (Fig. 8b) shows that ALBATROSS achieves similarly good agreement with the frostpoint hygrometer in the troposphere (2–12 km altitude), with a mean deviation between ALBATROSS and CFH of –1 ± 8 %, and 82 % of the data points falling within ±10 %. The spread of the ALBATROSS – CFH differences in the upper troposphere can be partly attributed to atmospheric variability effects, as most of this comparison is based on tandem flights, in which the two instruments sampled air masses that increasingly diverged with altitude (see Section 4.1). Table 2 shows that the standard deviation of ALBATROSS – CFH between 8 and 12 km altitude decreases from 10 % in tandem flights (F0-F3) to 5 % considering co-located flights only (F4-F6).

In the stratosphere, despite the limited number of valid measurements, the results demonstrate that ALBATROSS consistently achieves agreement within the uncertainty range of CFH (±10 %: Vömel et al., 2007) up to 28 km altitude (~15 hPa pressure). The largest relative deviations are found in the tropopause region (12–16 km altitude), with standard deviations ~15 %, which is expected due to the combination of extremely low H_2O mixing ratios, strong vertical gradients, and differences in response

https://doi.org/10.5194/egusphere-2026-4762
Preprint. Discussion started: 25 August 2026

time between the two instruments. Above this range, and particularly between 16 and 24 km altitude, the agreement between ALBATROSS and CFH demonstrates the ability of the laser spectrometer to accurately and precisely resolve lower-stratospheric H_2O mixing ratios in the 4–6 ppm range (mean deviation 3 ± 3 % for 16–28 km: Table 2). Averaged over all valid stratospheric measurements (altitudes 12–28 km), the mean ± standard deviation of ALBATROSS – CFH is 3 ± 10 %, with 83 % of the measurements falling in the ±10 % deviation range.

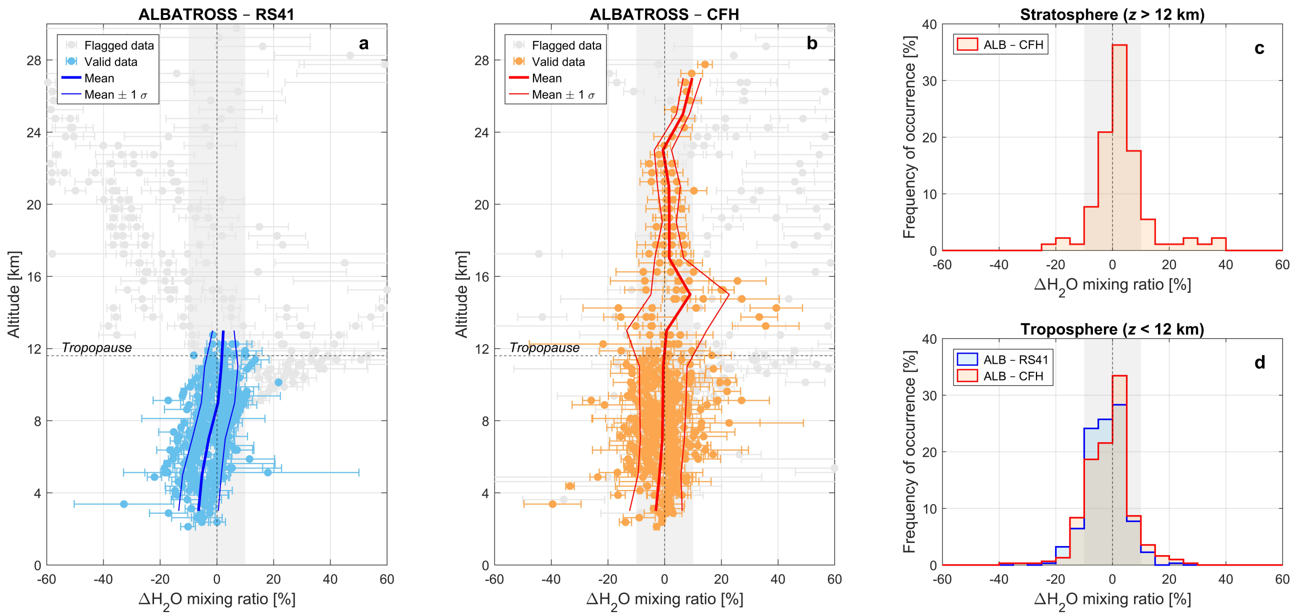

Figure 8. Statistical comparison. Panels (a-b): scatter plots of the relative difference (ΔH_2O) of ALBATROSS – RS41 (panel a) and ALBATROSS – CFH (b), as a function of altitude, for all flights (both ascent and descent data). Valid measurements are shown as colored dots and flagged data points as grey dots. Blue (red) solid lines in panels a (b) represent the mean (thick line) and mean ± standard deviation range (thin lines) of ΔH_2O calculated in 2 km layers. Black dashed lines indicate the average tropopause altitude of all flights (11.8 km). Panels (c-d): frequency of occurrence distributions of ΔH_2O for ALBATROSS – CFH (red) and ALBATROSS – RS41 (blue), calculated for all measurements in the stratosphere (z > 12 km, panel c) and troposphere (z < 12 km, panel d).

5. Conclusions

We have presented the first comprehensive in-flight validation of ALBATROSS, a compact (3.6 kg), balloon-borne laser absorption spectrometer developed for high-accuracy measurements of H_2O in the UTLS. The validation was based on seven balloon flights performed between 2022 and 2026 from the meteorological observatories of Lindenberg, Germany (one flight) and Payerne, Switzerland (six flights), featuring simultaneous measurements by established reference instruments, such as the cryogenic frostpoint hygrometer (CFH) and the Vaisala RS41 radiosonde.

https://doi.org/10.5194/egusphere-2026-4762
Preprint. Discussion started: 25 August 2026

Altitude range	**ALBATROSS – RS41**	**ALBATROSS – CFH**		
	All flights	Tandem flights (F0–F3)	Co-located flights (F4–F6)	All flights
Free troposphere (2–8 km)	–5 ± 7 % (203)	–1 ± 7 % (75)	–2 ± 8 % (99)	–2 ± 8 % (174)
Upper troposphere (8–12 km)	1 ± 6 % (139)	1 ± 10 % (74)	–2 ± 5 % (63)	–1 ± 8 % (137)
Troposphere (2–12 km)	**–2 ± 7 % (342)**	**0 ± 9 % (149)**	**–2 ± 7 % (162)**	**–1 ± 8 % (311)**
Tropopause region (12–16 km)	-	4 ± 6 % (12)	5 ± 17 % (24)	5 ± 14 % (36)
Lower stratosphere (16–28 km)	-	0 ± 2 % (13)	3 ± 3 % (42)	3 ± 3 % (55)
Stratosphere (12–28 km)	**-**	**3 ± 6 % (25)**	**4 ± 11 % (66)**	**3 ± 10 % (91)**

Table 2. Statistical comparison summary: mean ± 1 σ standard deviation of ALBATROSS – RS41 and ALBATROSS – CFH, calculated over four atmospherically relevant altitude ranges. For ALBATROSS – CFH, the deviations are calculated for all flights, as well as for tandem (F0-F3) and co-located flights (F4-F6) separately. For ALBATROSS – RS41, all flights are co-located (see Table 1). Values in parentheses indicate the number of valid data points considered for each comparison and altitude range.

The results demonstrate that ALBATROSS achieves accurate and statistically robust water vapor measurements in the troposphere, with mean relative differences of –2 ± 7 % with respect to RS41 and –1 ± 8 % with respect to CFH below 12 km altitude, and more than 80 % of the data falling within deviations of ±10 % relative to both reference instruments. This level of agreement is maintained over about three orders of magnitude in H_2O mixing ratio (~5–5000 ppm), while fine-scale vertical structures are consistently resolved, including measurements within cirrus cloud layers.

In the stratosphere, following iterative mitigation of internal contamination effects, ALBATROSS achieves accurate and high-resolution measurements of H_2O mixing ratio up to 28 km altitude (15 hPa). Valid stratospheric profiles, obtained in four out of seven validation flights, show agreement within ±10 % relative to CFH for more than 80 % of individual data points. Statistical analysis of all valid stratospheric measurements yields a mean relative deviation of 3 ± 10 % between ALBATROSS and CFH in the 12–28 km altitude range. The largest relative differences are found in the tropopause region (12–16 km), while substantially lower scatter is obtained in the lower stratosphere (mean deviation 3 ± 3 % for 16–28 km altitude), demonstrating the ability of the laser spectrometer to accurately and precisely resolve H_2O mixing ratios in the 4–6 ppm range.

A key advantage of the laser spectroscopy technique is highlighted by the analysis of two "balloon spikes" observed simultaneously by ALBATROSS and CFH in the stratosphere during flight F4. These transient events demonstrate the substantially faster dynamic response of ALBATROSS (response time ~1 s, corresponding to 5 m effective vertical resolution) compared to CFH (response time 3–4 s, effective vertical resolution 15–20 m). The fast response of the laser spectrometer allows a faithful representation of small-scale perturbations in UTLS H_2O and highlights the potential of this technique to complement and, in specific aspects, exceed the performance of chilled-mirror hygrometers.

https://doi.org/10.5194/egusphere-2026-4762
Preprint. Discussion started: 25 August 2026

The validation campaign also revealed technical challenges inherent to open-path balloon-borne laser spectroscopy, most notably the contamination arising from internal moisture within the instrument's enclosure, and the different pathways by which this can affect the measurements (see Section 2.2). These effects were physically understood, independently diagnosed using housekeeping data (e.g., interruptions of purge gas flow caused by dry-ice formation in the release system), and largely mitigated through targeted design improvements. Consequently, the present analysis also provides valuable insight into the operational requirements and reliability constraints for routine UTLS deployments.

Overall, this work establishes mid-infrared laser spectroscopy as a viable reference-quality technique for balloon-borne measurements of UTLS water vapor, combining SI-traceable accuracy, high vertical resolution, and fast response, in a lightweight instrument (ALBATROSS). In the context of declining satellite coverage and ongoing transitions in frostpoint hygrometry technology, laser absorption spectroscopy represents a highly promising approach for long-term UTLS monitoring.

Data availability

The data will be uploaded to a public data repository (DOI will be added).

Supplement

The supplement related to this article is available online at:

Author contributions

SB coordinated the ALBATROSS flights, operated the spectrometer, analyzed the data, and wrote the paper with contributions from all authors. YP operated the CFH instrument in the Payerne flights and supported the data analysis. PS and BT provided hardware and software support for ALBATROSS development. GR, YP, AW, AF, AB, GM, FGW, TP, AH, LE, GS and BT supported the realization of the balloon flights in Payerne. PO and RD supported the realization of the balloon flight in Lindenberg. BT and GS supervised the project.

Competing interests

The authors declare that they have no conflict of interests.

Acknowledgements

We gratefully acknowledge technical support by the radiosounding teams of MeteoSwiss at Payerne and DWD at Lindenberg. The authors thank Hannes Wäckerlig (Empa), Alain Rey (MeteoSwiss), Vivienne Artho (ETH Zürich), Killian Brennan (University of Bern), Steven Brossi, Thomas Brossi (mylab electronik GmbH), and Susanne Meier (DWD) for support in balloon flights preparation and payload recovery; Julian Gisler (Empa) for support in generating of the graphics of Figs. 1a and 2c; Herbert Looser (Empa) for continuous software support.

https://doi.org/10.5194/egusphere-2026-4762
Preprint. Discussion started: 25 August 2026

Financial support

This work was supported by the Swiss Federal Office of Meteorology and Climatology (MeteoSwiss) in the framework of the Global Atmospheric Watch (GAW) / Global Climate Observing System (GCOS) Switzerland (GAW/GCOS-CH) Programme, within the project "Swiss H_2O Hub" (https://www.meteoswiss.admin.ch/about-us/research-and-cooperation/programmes-gaw-ch-and-gcos-ch/gaw-ch-and-gcos-ch-supported-activities.html, last access: 6 August 2026).

References

Brunamonti, S., Jorge, T., Oelsner, P., Hanumanthu, S., Singh, B. B., Kumar, K. R., Sonbawne, S., Meier, S., Singh, D., Wienhold, F. G., Luo, B. P., Boettcher, M., Poltera, Y., Jauhiainen, H., Kayastha, R., Karmacharya, J., Dirksen, R., Naja, M., Rex, M., Fadnavis, S., and Peter, T.: Balloon-borne measurements of temperature, water vapor, ozone and aerosol backscatter on the southern slopes of the Himalayas during StratoClim 2016–2017, Atmos. Chem. Phys., 18, 15937–15957, https://doi.org/10.5194/acp-18-15937-2018, 2018.

Brunamonti, S., Füzér, L., Jorge, T., Poltera, Y., Oelsner, P., Meier, S., Dirksen, R., Naja, M., Fadnavis, S., Karmacharya, J., Wienhold, F. G., Luo, B. P., Wernli, H., and Peter, T.: Water Vapor in the Asian Summer Monsoon Anticyclone: Comparison of Balloon-Borne Measurements and ECMWF Data, J. Geophys. Res.-Atmos., 124, 7053–7068, https://doi.org/10.1029/2018JD030000, 2019.

Brunamonti, S., Graf, M., Bühlmann, T., Pascale, C., Ilak, I., Emmenegger, L., and Tuzson, B.: SI-traceable validation of a laser spectrometer for balloon-borne measurements of water vapor in the upper atmosphere, Atmos. Meas. Tech., 16, 4391–4407, https://doi.org/10.5194/amt-16-4391-2023, 2023.

Brunamonti, S., Saathoff, H., Hertzog, A., Diskin, G., Fujiwara, M., Rosenlof, K., Möhler, O., Tuzson, B., Emmenegger, L., Amarouche, N., Durry, G., Frérot, F., Samake, J.-C., Cenac, C., Lopez, J., Monnier, P., and Ghysels, M.: The AquaVIT-4 intercomparison of atmospheric hygrometers, Atmos. Meas. Tech., 18, 5321–5348, https://doi.org/10.5194/amt-18-5321-2025, 2025.

Dirksen, R: R23 replacement (HP-2), 15th GRUAN Implementation and Coordination Meeting (ICM-15), Bern, Switzerland, 11-15 March 2024, https://www.gruan.org/gruan/editor/documents/meetings/icm-15/pres/pres_0610b_Dirksen_R23.pdf (last access: 3 August 2026), 2024.

Durry, G., Amarouche, N., Joly, L., Liu, X., Parvitte, B., and Zéninari, V.: Laser diode spectroscopy of H_2O at 2.63 µm for atmospheric applications, Appl. Phys. B-Lasers O., 90, 573–580, https://doi.org/10.1007/s00340-007-2884-3, 2008.

Fahey, D. W., Gao, R.-S., Möhler, O., Saathoff, H., Schiller, C., Ebert, V., Krämer, M., Peter, T., Amarouche, N., Avallone, L. M., Bauer, R., Bozóki, Z., Christensen, L. E., Davis, S. M., Durry, G., Dyroff, C., Herman, R. L., Hunsmann, S., Khaykin, S. M., Mackrodt, P., Meyer, J., Smith, J. B., Spelten, N., Troy, R. F., Vömel, H., Wagner, S., and Wienhold, F. G.: The AquaVIT-1 intercomparison of atmospheric water vapor measurement techniques, Atmos. Meas. Tech., 7, 3177–3213, https://doi.org/10.5194/amt-7-3177-2014, 2014.

https://doi.org/10.5194/egusphere-2026-4762
Preprint. Discussion started: 25 August 2026

Fischer, M., Tuzson, B., Hugi, A., Brönnimann, R., Kunz, A., Blaser, S., Rochat, M., Landry, O., Müller, A., and Emmenegger, L.: Intermittent operation of QC-lasers for mid-IR spectroscopy with low heat dissipation: tuning characteristics and driving electronics, Opt. Express, 22, 7014–7027, https://doi.org/10.1364/OE.22.007014, 2014.

Forster, P., Storelvmo, T., Armour, K., Collins, W., Dufresne, J.-L., Frame, D., Lunt, D. J., Mauritsen, T., Palmer, M. D., Watanabe, M., Wild, M., and Zhang, H.: The Earth's Energy Budget, Climate Feedbacks, and Climate Sensitivity, in: Climate Change 2021: The Physical Science Basis, Contribution of Working Group I to the Sixth Assessment Report of the Intergovernmental Panel on Climate Change, edited by: Masson-Delmotte, V., Zhai, P., Pirani, A., Connors, S. L., Péan, C., Berger, S., Caud, N., Chen, Y., Goldfarb, L., Gomis, M. I., Huang, M., Leitzell, K., Lonnoy, E., Matthews, J. B. R., Maycock, T. K., Waterfield, T., Yelekçi, O., Yu, R., and Zhou, B., Cambridge University Press, Cambridge, UK and New York, NY, USA, 923–1054, https://doi.org/10.1017/9781009157896.009, 2021.

GCOS: The 2022 GCOS ECVs Requirements - Updated in 2025, GCOS Report-245, https://library.wmo.int/idurl/4/58111 (last access: 3 August 2026), 2025.

Ghysels, M., Riviere, E. D., Khaykin, S., Stoeffler, C., Amarouche, N., Pommereau, J.-P., Held, G., and Durry, G.: Intercomparison of in situ water vapor balloon-borne measurements from Pico-SDLA H2O and FLASH-B in the tropical UTLS, Atmos. Meas. Tech., 9, 1207–1219, https://doi.org/10.5194/amt-9-1207-2016, 2016.

Ghysels, M., Durry, G., Amarouche, N., Hurst, D., Hall, E., Xiong, K., Dupont, J.-C., Samake, J.-C., Frérot, F., Bejjani, R., and Riviere, E. D.: Pico-Light H2O: intercomparison of in situ water vapour measurements during the AsA 2022 campaign, Atmos. Meas. Tech., 17, 3495–3513, https://doi.org/10.5194/amt-17-3495-2024, 2024.

Graf, M., Emmenegger, L., and Tuzson, B.: Compact, circular, and optically stable multipass cell for mobile laser absorption spectroscopy, Opt. Lett., 43, 2434–2437, https://doi.org/10.1364/OL.43.002434, 2018.

Graf, M., Scheidegger, P., Kupferschmid, A., Looser, H., Peter, T., Dirksen, R., Emmenegger, L., and Tuzson, B.: Compact and lightweight mid-infrared laser spectrometer for balloon-borne water vapor measurements in the UTLS, Atmos. Meas. Tech., 14, 1365–1378, https://doi.org/10.5194/amt-14-1365-2021, 2021.

Hall, E. G., Jordan, A. F., Hurst, D. F., Oltmans, S. J., Vömel, H., Kühnreich, B., and Ebert, V.: Advancements, measurement uncertainties, and recent comparisons of the NOAA frost point hygrometer, Atmos. Meas. Tech., 9, 4295–4310, https://doi.org/10.5194/amt-9-4295-2016, 2016.

Hardy, B.: ITS-90 Formulations for vapor pressure, frostpoint temperature, dewpoint temperature, and enhancement factors in the range –100 to +100 °C. The Proceedings of the Third International Symposium on Humidity & Moisture, London, England, 1998.

Hegglin, M. I., Tegtmeier, S., Anderson, J., Froidevaux, L., Fuller, R., Funke, B., Jones, A., Lingenfelser, G., Lumpe, J., Pendlebury, D., Remsberg, E., Rozanov, A., Toohey, M., Urban, J., von Clarmann, T., Walker, K. A., Wang, R., and Weigel, K.: SPARC Data Initiative: Comparison of water vapor climatologies from international satellite limb sounders. J. Geophys. Res.-Atmos., 118, 11,824–11,846, https://doi.org/10.1002/jgrd.50752, 2013.

https://doi.org/10.5194/egusphere-2026-4762
Preprint. Discussion started: 25 August 2026

Hurst, D. F., Oltmans, S. J., Vömel, H., Rosenlof, K. H., Davis, S. M., Ray, E. A., Hall, E. G., and Jordan, A. F.: Stratospheric water vapor trends over Boulder, Colorado: Analysis of the 30 year Boulder record, J. Geophys. Res.-Atmos., 116, D02306, https://doi.org/10.1029/2010JD015065, 2011.

Hurst, D., Lambert, A., Read, B., Davis, S., Rosenlof, K., Hall, E., Jordan, A., and Oltmans, S.: Validation of Aura Microwave Limb Sounder stratospheric water vapor measurements by the NOAA frost point hygrometer, J. Geophys. Res., 119, 1612-1625, doi:10.1002/2013JD020757, 2014.

Hurst, D. F., Read, W. G., Vömel, H., Selkirk, H. B., Rosenlof, K. H., Davis, S. M., Hall, E. G., Jordan, A. F., and Oltmans, S. J.: Recent divergences in stratospheric water vapor measurements by frost point hygrometers and the Aura Microwave Limb Sounder, Atmos. Meas. Tech., 9, 4447–4457, https://doi.org/10.5194/amt-9-4447-2016, 2016.

Jorge, T., Wienhold, F. G., Germann, N., Weers, U., Vecellio, M., Brossi, S., Brossi, T., Krieger, U. and Peter, T.: PCFH – Peltier Cooled Frost point Hygrometer, 12th GRUAN Implementation and Coordination Meeting (ICM-12), Virtual Session, 16-20 November 2020, https://www.gruan.org/gruan/editor/documents/meetings/icm-12/pres/pres_303_Jorge_PCFH.pdf (last access: 3 August 2026), 2020.

Jorge, T., Brunamonti, S., Poltera, Y., Wienhold, F. G., Luo, B. P., Oelsner, P., Hanumanthu, S., Singh, B. B., Körner, S.,1590 Dirksen, R., Naja, M., Fadnavis, S. and Peter, T.: Understanding balloon-borne frost point hygrometer measurements after contamination by mixed-phase clouds, Atmos. Meas. Tech., 14(1), 239–268, https://doi.org/10.5194/amt-14-239-2021, 2021.

Khaykin, S., Podglajen, A., Ploeger, F., Grooß, J.-U., Tence, F., Bekki, S., Khlopenkov, K., Bedka, K., Rieger, L., Baron, A., Godin-Beekmann, S., Legras, B., Sellitto, P., Sakai, T., Barnes, J., Uchino, O., Morino, I., Nagai, T., Wing, R., Baumgarten, G., Gerding, M., Duflot, V., Payen, G., Jumelet, J., Querel, R., Liley, B., Bourassa, A., Clouser, B., Feofilov, A., Hauchecorne, A., and Ravetta, F.: Global perturbation of stratospheric water and aerosol burden by Hunga eruption., Commun. Earth Environ. 3, 316, https://doi.org/10.1038/s43247-022-00652-x, 2022.

Liu, C., Tuzson, B., Scheidegger, P., Looser, H., Bereiter, B., Graf, M., Hundt, M., Aseev, O., Maas, D., and Emmenegger, L.: Laser driving and data processing concept for mobile trace gas sensing: Design and implementation, Rev. Sci. Instrum., 89, 065107, https://doi.org/10.1063/1.5026546, 2018.

Luo, B. P., Peter T., Fueglistaler, S., Wernli, H., Wirth, M., Kiemle, C., Flentje, H., Yushkov, V. A., Khattatov, V., Rudakov, V., Thomas, A., Borrmann, S., Toci, G., Mazzinghi, P., Beuermann, J., Schiller, C., Cairo, F., Di Donfrancesco, G., Adriani, A., Volk, C. M., Strom, J., Noone, K., Mitev, V., MacKenzie, R. A., Carslaw, K. S., Trautmann, T., Santacesaria, V., and Stefanutti, L.: Dehydration potential of ultrathin clouds at the tropical tropopause, Geophys. Res. Lett., 30, 1557, https://doi.org/10.1029/2002GL016737, 2003.

Maycock, A. C., Joshi, M. M., Shine, K. P., Davis, S. M., and Rosenlof, K. H.: The potential impact of changes in lower stratospheric water vapour on stratospheric temperatures over the past 30 years, Q. J. R. Meteorol. Soc., 140, 684, 2176-2185, https://doi.org/10.1002/qj.2287, 2014

https://doi.org/10.5194/egusphere-2026-4762
Preprint. Discussion started: 25 August 2026

Meyer, J., Rolf, C., Schiller, C., Rohs, S., Spelten, N., Afchine, A., Zöger, M., Sitnikov, N., Thornberry, T. D., Rollins, A. W., Bozóki, Z., Tátrai, D., Ebert, V., Kühnreich, B., Mackrodt, P., Möhler, O., Saathoff, H., Rosenlof, K. H., and Krämer, M.: Two decades of water vapor measurements with the FISH fluorescence hygrometer: a review, Atmos. Chem. Phys., 15, 8521–8538, https://doi.org/10.5194/acp-15-8521-2015, 2015.

Murphy, D.M., and Koop, T.: Review of the vapour pressures of ice and supercooled water for atmospheric applications, Q.J.R. Meteorol. Soc., 131: 1539-1565, https://doi.org/10.1256/qj.04.94, 2005.

Oltmans, S., Rosenlof, K., Michelsen, H., Nedoluha, G., Pan, L., Read, W., Remsberg, E., and Schiller, C.: SPARC Report No. 2: Upper Tropospheric and Stratospheric Water Vapour, Chap. 2, Tech. rep., https://aparc-climate.org/publications/sparc-report-no-2/ (last access: 3 August 2026), 2000.

Poltera, Y., Luo, B., Wienhold, F. G., and Peter, T.: The “Golden Points” and nonequilibrium correction of high-accuracy frost point hygrometers, Atmos. Meas. Tech., 19, 5091–5134, https://doi.org/10.5194/amt-19-5091-2026, 2026.

Reinares Martínez, I., Evan, S., Wienhold, F. G., Brioude, J., Jensen, E. J., Thornberry, T. D., Héron, D., Verreyken, B., Körner, S., Vömel, H., Metzger, J.-M., and Posny, F.: Unprecedented observations of a nascent in situ cirrus in the tropical tropopause layer, Geophys. Res. Lett., 48, e2020GL090936, https://doi.org/10.1029/2020GL090936, 2020.

Riese, M., Ploeger, F., Rap, A., Vogel, B., Konopka, P., Dameris, M., and Forster, P.: Impacts of uncertainties in atmospheric mixing on simulated UTLS composition and related radiative effects, J. Geophys. Res.-Atmos., 117, D16305, https://doi.org/10.1029/2012JD017751, 2012.

Rolf, C., Khordakova, D., and Vömel, H.: CFH cooling agent alternatives, 12th GRUAN Implementation and Coordination Meeting (ICM-12), Virtual Session, 16-20 November 2020, https://www.gruan.org/gruan/editor/documents/meetings/icm-12/pres/pres_302_Rolf_CFH_Cooling-Agent-Tests.pdf (last access: 3 August 2026), 2020.

Rollins, A. W., Thornberry, T., Gao, R. S., Smith, J. B., Sayres, D. S., Sargent, M. R., Schiller, C., Krämer, M., Spelten, N., Hurst, D. F., Jordan, A. F., Hall, E. G., Vömel, H., Diskin, G. S., Podolske, J. R., Christensen, L. E., Rosenlof, K. H., Jensen, E. J., and Fahey, D. W.: Evaluation of UT/LS hygrometer accuracy by intercomparison during the NASA MAC-PEX mission, J. Geophys. Res.-Atmos., 119, 1915–1935, https://doi.org/10.1002/2013JD020817, 2014.

Salawitch, R. J., Smith, J. B., Selkirk, H., Wargan, K., Chipperfield, M. P., Hossaini, R., Levelt, P. F., Livesey, N. J., McBride, L. A., Millán, L. F., Moyer, E., Santee, M. L., Schoeberl, M. R., Solomon, S., Stone, K., and Worden, H. M.: The Imminent Data Desert: The Future of Stratospheric Monitoring in a Rapidly Changing World, Bull. Amer. Meteor. Soc., 106, E540–E563, https://doi.org/10.1175/BAMS-D-23-0281.1, 2025.

Santee, M. L., Manney, G. L., Livesey, N. J., Schwartz, M. J., Neu, J. L., and Read, W. G.: A comprehensive overview of the climatological composition of the Asian summer monsoon anticyclone based on 10 years of Aura Microwave Limb Sounder measurements, J. Geophys. Res. Atmos., 122, 5491–5514, doi:10.1002/2016JD026408, 2017.

Singer, C. E., Clouser, B. W., Khaykin, S. M., Krämer, M., Cairo, F., Peter, T., Lykov, A., Rolf, C., Spelten, N., Afchine, A., Brunamonti, S., and Moyer, E. J.: Intercomparison of upper tropospheric and lower stratospheric water vapor measurements over the Asian Summer Monsoon during the StratoClim campaign, Atmos. Meas. Tech., 15, 4767–4783, https://doi.org/10.5194/amt-15-4767-2022, 2022.

Solomon, S., Rosenlof, K. H., Portmann, R. W., Daniel, J. S., Davis, S. M., Sanford, T. J., and Plattner, G.-K.: Contributions of stratospheric water vapor to decadal changes in the rate of global warming, Science, 327, 1219–1223, https://doi.org/10.1126/science.1182488, 2010.

Sprenger, M. and Wernli, H.: The LAGRANTO Lagrangian analysis tool – version 2.0, Geosci. Model Dev., 8, 2569–2586, https://doi.org/10.5194/gmd-8-2569-2015, 2015.

Stenke, A. and Grewe, V.: Simulation of stratospheric water vapor trends: impact on stratospheric ozone chemistry, Atmos. Chem. Phys., 5, 1257–1272, https://doi.org/10.5194/acp-5-1257-2005, 2005.

Sugidachi, T., Fujiwara, M., Shimizu, K., Ogino, S.-Y., Suzuki, J., and Dirksen, R. J.: Development of a Peltier-based chilled mirror hygrometer, SKYDEW, for tropospheric and lower-stratospheric water vapor measurements, Atmos. Meas. Tech., 18(2), 509–531, https://doi.org/10.5194/amt-18-509-2025, 2025.

Survo, P., Lehtinen, R. and Kauranen, J.: SI traceability of Vaisala radiosonde RS41 sounding data – calibration and uncertainty analysis, Proceedings of the WMO Technical Conference on Meteorological and Environmental Instruments and Methods of Observation (TECO 2014), Saint Petersburg, Russian Federation, 7-9 July 2014, https://library.wmo.int/viewer/53114/download?file=P2_7_Survo_SITraceabilityRS41Data.pdf&type=pdf (last access: 3 August 2026), 2014.

Tuzson, B., Graf, M., Ravelid, J., Scheidegger, P., Kupferschmid, A., Looser, H., Morales, R. P., and Emmenegger, L.: A compact QCL spectrometer for mobile, high-precision methane sensing aboard drones, Atmos. Meas. Tech., 13, 4715–4726, https://doi.org/10.5194/amt-13-4715-2020, 2020.

UNEP: Montreal Protocol – Kigali Amendment, chap. XXVII, 2. f. Amendment to the Montreal Protocol on Substances that Deplete the Ozone Layer, Kigali, Rwanda, https://treaties.un.org/doc/Treaties/2016/10/20161015%2003-23%20PM/Ch_XXVII-2.f-English%20and%20French.pdf (last access: 3 August 2026), 2016.

Vaisala: Radiosonde RS41-SG Datasheet, https://docs.vaisala.com/v/u/B211321EN-L/en-US (last access: 3 August 2026), 2024.

Vömel, H., David, D. E., and Smith, K.: Accuracy of tropospheric and stratospheric water vapor measurements by the cryogenic frost point hygrometer: Instrumental details and observations, J. Geophys. Res.-Atmos., 112, D08305, https://doi.org/10.1029/2006JD007224, 2007.

Vömel, H., Naebert, T., Dirksen, R., and Sommer, M.: An update on the uncertainties of water vapor measurements using cryogenic frost point hygrometers, Atmos. Meas. Tech., 9, 3755–3768, https://doi.org/10.5194/amt-9-3755-2016, 2016.

Vömel, H., Evan, S., and Tully, M.: Water vapor injection into the stratosphere by Hunga Tonga-Hunga Ha'apai, Science, 377, 1444-1447, DOI:10.1126/science.abq2299, 2022.

Wang, J., Wang, Z., and Sun, B.: Improved equation of CO2 Joule–Thomson coefficient, Journal of CO2 Utilization, 19, 296-307, https://doi.org/10.1016/j.jcou.2017.04.007, 2017.

https://doi.org/10.5194/egusphere-2026-4762
Preprint. Discussion started: 25 August 2026

Wexler, A.: Vapor pressure formulation for water in range 0 to 100°C. A Revision, Journal of Research of the National Bureau of Standards, 80A(5-6), 775–785. https://doi.org/10.6028/jres.080A.071, 1976.

Zöger, M., Afchine, A., Eicke, N., Gerhards, M.-T., Klein, E., McKenna, D. S., Mörschel, U., Schmidt, U., Tan, V., Tuitjer, F., Woyke, T., and Schiller, C.: Fast in situ stratospheric hygrometers: A new family of balloon-borne Lyman α photofragment fluorescence hygrometers, J. Geophys. Res., 104, 1807–1816, 1999.